Controllable optical multi-well trap and its optical lattices using compounded cosine patterns*

Zhou Qi(周 琦)[a)b)], Lu Jun-Fa(陆俊发)[b)], and Yin Jian-Ping(印建平)[a)†]

[a)] *Key Laboratory of Optical and Magnetic Resonance Spectroscopy, Ministry of Education, Department of Physics, East China Normal University, Shanghai* 200062, *China*

[b)] *Department of Physics, East China Institute of Technology, Fuzhou* 344000, *Jiangxi Province, China*

(Received 26 March 2010; revised manuscript received 10 July 2010)

This paper proposes a flexible scheme to form various optical multi-well traps for cold atoms or molecules by using a simple optical system composed of an compounded amplitude cosine-only grating and a single lens illuminated by a plane light wave or a Gaussian beam. Dynamic manipulation and evolution of multi-well trap can be easily implemented by controlling the modulation frequency of the cosine patterns. It also discusses how to expand this multi-well trap to two-dimensional lattices with single- or multi-well trap by using an orthogonally or non-orthogonally modulated grating, as well as using incoherent multi-beam illumination, and these results show that all the symmetric structures of two-dimensional Bravais lattices can be obtained facilely by using proposed scheme.

Keywords: multi-well optical trap, optical lattices, amplitude cosine-only grating, spatial light modulator

PACC: 3280P, 4225F

1. Introduction

Since optical lattices, periodic arrays of atoms bound by light, came to the world in 1991–1992,[1,2] it has provided a perfect physical platform for studies of atomic trapping and cooling, atomic or molecular Bose–Einstein condensation,[3−5] as well as some foundational phenomena in condensed matter, like Bloch oscillations,[6] Wannier–Stark ladders,[7] photonic band gaps,[8−10] and so on, due to the similarity between optical lattices and solid crystals. In conventional standing-wave lattices, the lattice constant is about several hundred nanometers, which is in the order of the laser wavelength. Such small separation of the individual trapping sites leads to a small trapping volume and a few trapped atoms. More importantly, it is hard to implement the precise manipulation of individual trapping sites in such lattices, which is especially significant for quantum information processing, such as the capability of initializing, addressing and reading out the qubits. Furthermore, there is still an intensive search for the multi-species collisions,[11] entanglement,[12,13] interference[14,15] and quantum gate operations of neutral atoms,[16] as well as quantum many particle systems.[17] All of these physical processes rely on a controllable multi-well system to realize atom–atom interactions or controlled collisions.

The important and versatile technology to obtain multiple trapping sites is holographic optical tweezers,[18,19] which allows a single beam to be transformed into various array of independent trapping sites in focal plane of single lens instead of a microlens array usually required in some micro-fabricated optical systems,[20−22] by using spatial light modulator (SLM). The technology of SLMs had been originally applied in colloidal physics experiments. The first theoretical discussion in the possibility of application of atomic optics has been made by D. McGloin and his co-workers in 2003.[23] Soon after, it has been implemented in experiments for static trapping and guiding cold atoms by many groups.[19,24−26] In recent years, the feasibility of dynamic spatial manipulation of cold atoms with high-speed SLMs or associated with SLMs and acousto-optic modulator have

*Project supported by the National Natural Science Foundation of China (Grant Nos. 10434060, 10674047 and 10804031), the National Key Basic Research and Development Program of China (Grant No. 2006CB921604), the Program for Changjiang Scholar and Innovative Research Team, and Shanghai Leading Academic Discipline Project (Grant No. B408), the Youth Foundation of Jiangxi Educational Committee (Grant No. GJJ09530), and the Open Research Fund of State Key Laboratory of Precision Spectroscopy, East China Normal University.

†Corresponding author. E-mail: jpyin@phy.ecnu.edu.cn

© 2010 Chinese Physical Society and IOP Publishing Ltd

also been proved.[26,27] In addition to trapping in two dimensions, currently, such applications have been extended to higher degree of spatial freedom through time-sharing potential[28] and dynamic manipulation of atom with high-speed ferroelectric SLM.

For most of the applications of SLMs, the generations of intensity pattern depend on the calculation of holograms, which is the fast Fourier transform (FFT) of the wave front at focal plane. This algorithm is generally discrete and iterative. After taking into account the effect of performance of display device, the wanted fields may suffer from a larger distortion. In this paper, our object is located at creating special trapping potential of cold atoms, such as multiple-well and periodic lattice trap, and we attempt to start our discussion from finding relation between the cosine grating and the intensity profiles at the focal plane, which is simple and well known. Regarding this pattern as a basic element and combine them with some special rules, we can obtain the complex intensity profiles directly without any FFT. Combining with non-orthogonally modulation and multi-beam illumination, we present how to obtain all types of two-dimensional (2D) optical Bravais lattices, even including compound lattices and lattices with periodic defects.

The paper is organized as follows. The proposed scheme to form a multi-well optical trap is presented in Section 2. In Section 3, a double-well optical trap is discussed in some detail. Also, a continuous reversible evolution between a double-well trap and a single-well one is discussed. In Section 4, various 2D optical lattices with a single- or multi-well trap are proposed for further applications. Some main results and conclusions are included in the final section.

2. Scheme of controllable optical multi-well trap

A proposed scheme to form a controllable optical one-dimensional (1D) four-well trap is shown in Fig. 1(a). We consider a plane light wave (or a collimated Gaussian beam with a TEM_{00} mode) perpendicularly passed through our optical system along the z axis, and the used optical system is composed of an amplitude cosine-only grating and a rectangular positive lens with a side length $2a$ and a focal length f. The transmissivity of the amplitude cosine-only grating is modulated spatially by $\cos(2\pi vx)\times\cos[2\pi(2v)x]$, and its grating pattern is shown in Fig. 1(b). Here, the SLM consisted of a programmable liquid crystal device (LCD) is working on the mode of amplitude modulation and acts as a cosine grating. Each pixel is controlled individually by using a video graphics array (VGA) signal from a computer. The intensity of incident light is modulated by a prescribed cosine pattern displayed on the LCD. It also becomes possible for real-time and continuous control by rapidly refreshing this pattern.

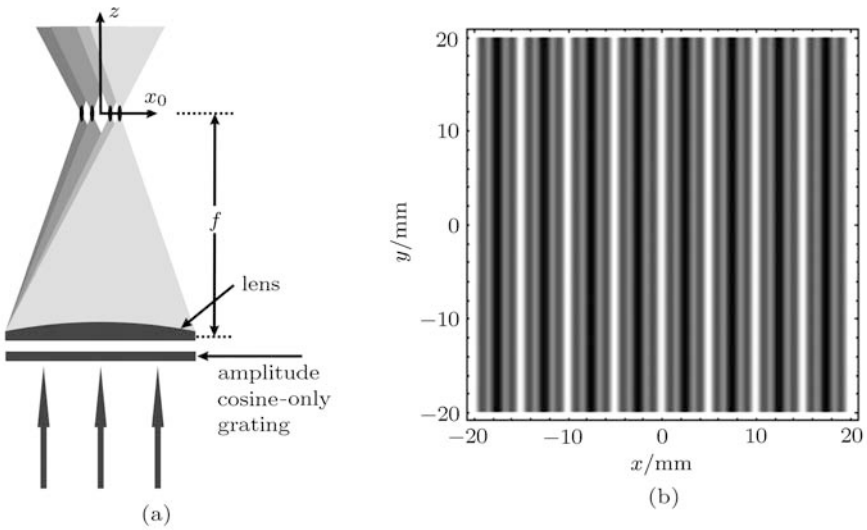


Fig. 1. (a) Schematic diagram of forming an optical four- or multi-well trap for cold atoms or molecules. (b) An example of the grating pattern modulated by $\cos(2\pi vx)\cos[2\pi(2v)x]$ with a spatial frequency of $v = 0.2$ mm^{-1}.

The distribution of light field in the focal plane, such as the x_0oy_0 plane at the position of $z = f$, is

determined by Fresnel diffraction of the lens aperture when the grating is absent. After taking account of the contribution of the grating, the resulting field should be a convolution of the aperture diffraction and the Fourier transformation of the modulation functions (two δ functions correspond to one cosine function), and then the four focal points (i.e., four optical wells) will be formed in the x_0oy_0 plane. Figure 2 shows the 2D gray map of intensity distribution in the x_0oy_0 plane [Fig. 2(a)] and the x_0oz plane [Fig. 2(b)], respectively. When the input laser is detuned to the red of the atomic resonance frequency, these focused points can be used to trap cold atoms or molecules due to AC Stark effect. Our further analysis indicates that the separation of trapping centres is related directly to the space frequency v of the cosine function, and a continuous reversible evolution between a multi-well trap and a single-well one can be implemented by changing v. More details about this evolution process will be discussed in Section 3.

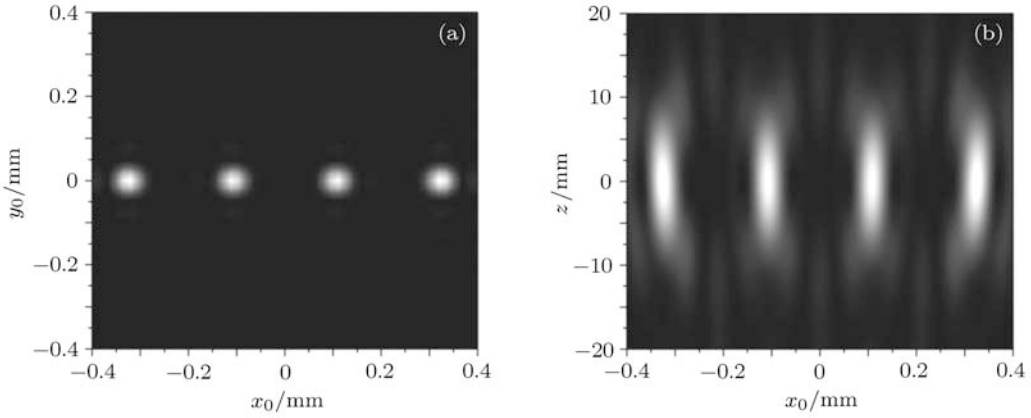


Fig. 2. The gray map of a four-well trap in (a) the x_0oy_0 plane and (b) the x_0oz plane, which is formed by the grating pattern shown in Fig. 1(b). For an intuitive view, the focal plane of the lens is chosen as $z = 0$ plane. The used parameters in the calculation are $a = 5$ mm, $f = 50$ cm, $\lambda = 1.06$ μm, $v = 0.2$ mm^{-1} and the intensity of incident light is $I_o = 1.27 \times 10^5$ W/m^2.

Keeping the optical system unchanged and applying different modulated functions on the SLM, we can also generate various 1D or 2D multi-well traps, as shown in Fig. 3.

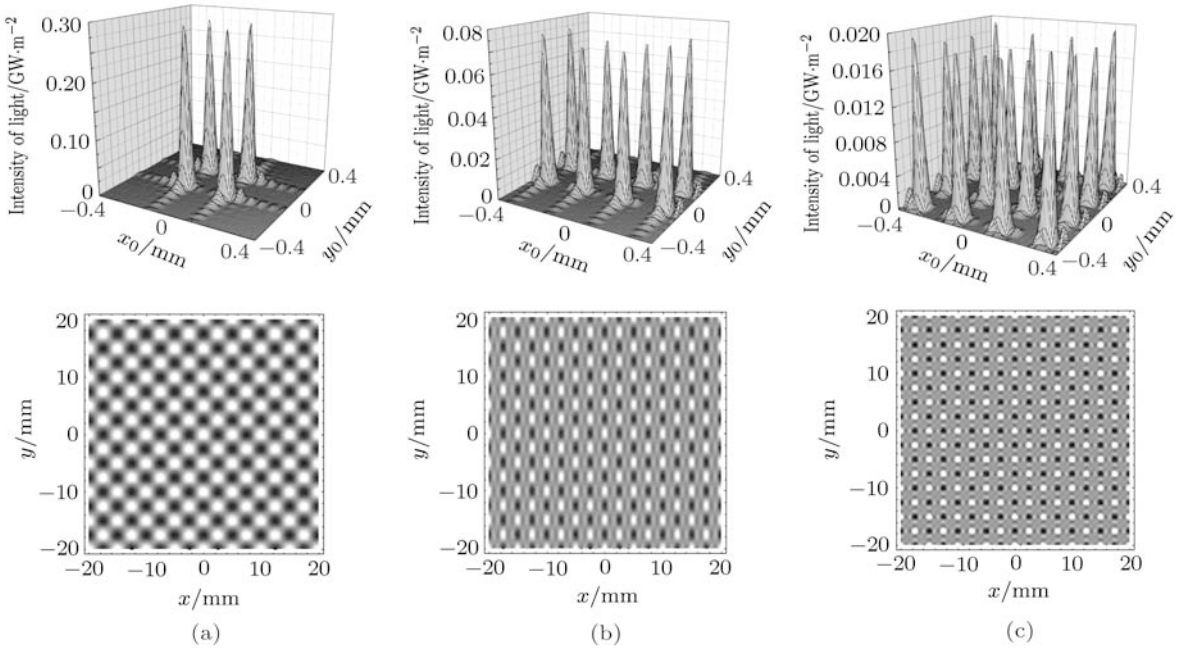


Fig. 3. (a) A 2×2 2D four-well trap generated by $\cos(2\pi vx) \times \cos(2\pi vy)$. (b) A 4×2 eight-well trap produced by $\cos(2\pi vx) \times \cos[2\pi(2v)x] \times \cos(2\pi vy)$. (c) A 4×4 sixteen-well trap generated by $\cos(2\pi vx) \times \cos[2\pi(2v)x] \times \cos(2\pi vy) \times \cos[2\pi(2v)y]$. The upper figures are the intensity distribution of multi-well trap in the x_0oy_0 plane, and the lower figures are the corresponding grating pattern. The parameters of optical system are the same as those in Fig. 2.

Expanding the modulation function to 2D space, we find that the functions of $\cos(2\pi vx) \times \cos(2\pi vy)$, $\cos(2\pi vx) \times \cos[2\pi(2v)x] \times \cos(2\pi vy)$ or $\cos(2\pi vx) \times \cos[2\pi(2v)x] \times \cos(2\pi vy) \times \cos[2\pi(2v)y]$ can generate a 2D multi-well traps with 2×2, 4×2 or 4×4 optical wells, respectively [see Fig. 3(a), 3(b) and 3(c)]. In these figures, the upper are the corresponding 2D intensity distributions of optical multi-well trap in the x_0oy_0 plane, and the lower are the corresponding grating patterns.

3. Optical double-well trap and its evolution

We first discuss the optical double-well trap, which is the simplest configuration implemented by our system. Some key relationships between cosine pattern and generated trap can be analytically solved, and can be expanded to the situation of multi-well trap since main characteristic parameters of individual optical well are determined by the relative aperture of the lens, while the grating parameter only influences on the spatial position of each optical well in both cases of double-well trap and multi-well trap.

3.1. Optical double-well trap

The coordinate system is also shown in Fig. 1, where the used amplitude grating is in the xoy plane (i.e., in the plane of $z = 0$), and the coordinate origin is located at the centre of the grating plane. When the distance between the lens and the grating is ignored, the amplitude transmission function of the grating is given by

$$g(x, y) = \cos 2\pi vx \cdot \mathrm{rect}\left(\frac{x}{2a}, \frac{y}{2a}\right), \tag{1}$$

where $\mathrm{rect}(x/2a, y/2a)$ denotes a 2D rectangular function determined by the aperture of the lens. Assuming that a single-mode plane light wave with a wavelength λ and an intensity I_0 illuminates our optical system, the intensity distribution of the diffraction light field in the focal plane (i.e. in the x_0oy_0 plane at $z = f$) can be written as

$$\begin{aligned} I_f(x_0, y_0) = {} & \frac{4a^4 I_0}{(\lambda f)^2}\left\{\frac{\sin[(2\pi a x_0)/(\lambda f) - 2\pi av]}{[(2\pi a x_0)/(\lambda f) - 2\pi av]}\right. \\ & \left. + \frac{\sin[(2\pi a x_0)/(\lambda f) + 2\pi av]}{[(2\pi a x_0)/(\lambda f) + 2\pi av]}\right\}^2 \\ & \times \frac{\sin^2[(2\pi a y_0)/(\lambda f)]}{[(2\pi a y_0)/(\lambda f)]^2}, \end{aligned} \tag{2}$$

which clearly shows two diffraction peaks denoted respectively by two sine functions in the brace. There are two symmetrical maximum values (i.e., the two trapping centres of our double-well trap) respectively located at $x_{0\max} = \pm v\lambda f$, $y_{0\max} = 0$, and have the equal magnitudes given by

$$I_{\max}(x_0, y_0, f) = 4a^4 I_0/(\lambda f)^2. \tag{3}$$

According to these equations, we can see that, for each optical well, the spatial position depends on the frequency v of the modulating function, while the geometric parameters are determined by the relative aperture of the lens. These two optical wells, due to sharing the same lens, have identical geometry even in the case of more complex modulating function. Notice that the secondary diffraction, as a diffraction noise, may influence on the trapping and manipulating of cold atoms or molecules. Fortunately, our calculation shows that the maximum intensity of secondary diffraction is lower than 5% of the maximum intensity of major wells, which basically satisfy the need of future experiments.

Table 1. Some analytic relationships between the geometric parameters of the optical double-well trap and ones of optical system (a, f, λ, I_0).

$\Delta x_{\max} = 2v\lambda f$	$\Delta x_{1/2} = \Delta y_{1/2} = 0.22147\lambda(f/a)$	$\Delta z_{1/2} = 0.58707\lambda(f/a)^2$
$\Delta x_{1/e^2} = \Delta y_{1/e^2} = 0.35\lambda(f/a)$	$\Delta z_{1/e^2} = 0.98316\lambda(f/a)^2$	$\Delta V_{1/2} = 0.120617\lambda^3(f/a)^4$
$\Delta V_{1/e^2} = 0.504486\lambda^3(f/a)^4$	$\left\lvert\frac{\partial I}{\partial x}\right\rvert_{\max} = \left\lvert\frac{\partial I}{\partial y}\right\rvert_{\max} = 13.5758\left(\frac{a}{\lambda f}\right)^3 I_0 a^2$	$\left\lvert\frac{\partial^2 I}{\partial x^2}\right\rvert_{\max} = \left\lvert\frac{\partial^2 I}{\partial y^2}\right\rvert_{\max} = 105.276\left(\frac{a}{\lambda f}\right)^4 I_0 a^2$

For more details, some analytic relationships between the geometric parameters of the optical double-well trap and ones of optical system (a, f, λ, I_0) have also been listed in Table 1. In this table, $\Delta x_{\max}$ is the distance between the two optical wells, which is only related to the frequency v of the modulating function as the wavelength of incident laser and the focal length of the lens are constants. The half width and $1/e^2$ width of individual well in three dimensions are denoted by $\Delta x_{1/2}$, $\Delta y_{1/2}$, $\Delta z_{1/2}$, and $\Delta x_{1/e^2}$, $\Delta y_{1/e^2}$, $\Delta z_{1/e^2}$,

respectively. The $\Delta V_{1/2}$ and $\Delta V_{1/e^2}$ are corresponding effective trapping volumes and calculated by regarding the shape of each optical well as an ideal ellipsoid. These relationships show that the radial and axial sizes of each optical well and its trapping volume (including the number and its density of the trapped particles, even its temperature) can be controlled effectively by changing the relative aperture $\beta = a/f$ of the lens. The β is also a major factor for influencing the motion of cold atoms or molecules in optical well.

It should be noticed that a plane-wave model is used in the above calculation, while an illumination system with a collimated TEM_{00}-mode Gaussian beam is more usual and feasible in practice. The difference between the two calculated results using a Gaussian-beam illumination and a plane-wave light one is large when the beam waist w_0 is small. However, when $w_0 \geq \sqrt{2}a$, the intensity distributions of the double-well trap formed by the Gaussian-beam illumination is very close to that formed by the plane-wave one, and the larger the beam waist w_0 is, the smaller the difference of the calculated results from two beam models is. Especially, the same maximum intensity will be obtained when $\bar{I}_{\mathrm{G}}/I_0 = 1 + 1.054\exp(-1.625a/w_0)$ is satisfied, where $\bar{I}_{\mathrm{G}}$ is the average intensity of Gaussian laser beam.

Figures 4(a) and 4(b) show the contours of the intensity distribution of our double wells in the focal plane and optical axial one paralleled to the x axis respectively for $a = 5$ mm, $f = 50$ cm, $\lambda = 1.06$ μm, $I_o = 1.27 \times 10^5$ W/m^2. In particular, when the above calculation parameters are used, the maximum intensity of each optical well is about 1.15 GW/m^2, and the corresponding trapping depth for ^{87}Rb atoms is about 168 μK, which is high enough to trap cold ^{87}Rb atoms with a temperature of $\sim$30 μK from a standard optical molasses.

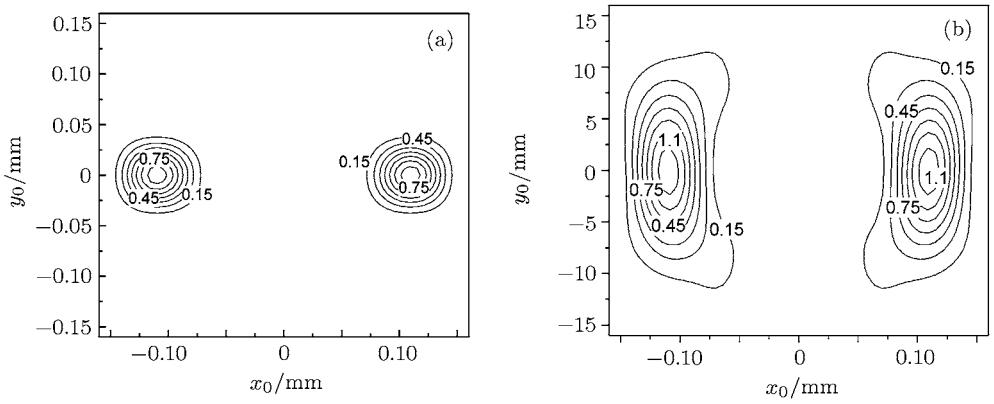


Fig. 4. A double-well trap generated by using a single cosine function with a space frequency of $v = 0.2$ mm^{-1} for $a = 5$ mm, $f = 50$ cm, $\lambda = 1.06$ μm, $I_o = 1.27 \times 10^5$ W/m^2. Figures (a) and (b) are the intensity contours of double-well trap in the x_0oy_0 and the x_0oz planes, respectively.

In our numerical calculation, there are slight differences of geometric parameters between those in x and y directions due to the influence of the secondary or higher order diffraction of another adjacent optical well in y directions. Choosing the boundary at $1/e^2$ width of each optical well, the averaged intensity $\overline{I}$ of each well can be estimated by calculating the integral of total trapping volume (i.e., $\Delta V_{1/e^2}$), and it is about 0.4283 GW/m^2. When the density n of cold particles in each optical well is 10^{12} $\sim 10^{14}$ cm^{-3}, the number of trapped particles N, can reach about 6.8×10^7 $\sim 6.8\times10^9$. Such a double-well trap has a broad prospect for application of all-optical atomic or molecular double-well BEC (Bose–Einstein condensate) by purely optical-potential evaporative cooling,[29] even to study cold collisions between two atomic or molecular samples if our double-well trap can be evolved as a single-well one, which will be discussed below.

3.2. Evolution of optical trap from double wells to a single well

In this subsection, we will show a continuous reversible evolution between a double-well trap and a single-well one. The analytic relationship between the separation $\Delta x_{\max}$ of two optical wells and the space frequency v of the cosine grating is given in Table 1, and $\Delta x_{\max}$ is proportional to the space frequency v. When the space

frequency v is reduced, two optical wells will be drawn close to each other, and a single-well trap will be formed ultimately as $v = 0.00$ mm^{-1}, just like the case without the grating.

Figures 5(a), 5(b) and 5(c) show the intensity contour distributions of our proposed optical trap when $v = 0.14$ mm^{-1}, 0.08 mm^{-1}, and 0.0 mm^{-1}, respectively. The amplitude of light field is modulated along the x direction, and the parameters used in the calculation are the same as those in Fig. 4. We can see from Fig. 5 that the optical trap will undergo a continuous evolvement from a two-well trap to a single-well one by reducing the space frequency v from 0.14 mm^{-1} to 0.0 mm^{-1}. In fact, as v decreases to a critical value $v_c = 0.064$ mm^{-1}, two wells are no longer distinguished from each other. When v is zero, the geometric parameters of the single-well trap in three directions are nearly the same as ones of the double-well trap, but their intensity gradients and their curvatures are far larger than ones of the double-well trap.

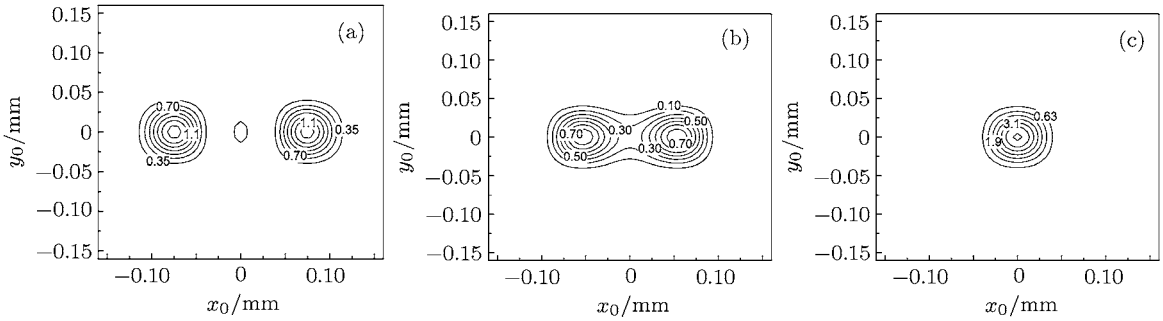


Fig. 5. Evolution of our optical trap from a double-well trap to a single-well one by reducing the modulation frequency v. The intensity contours of the optical trap are plotted in (a) for $v = 0.14$ mm^{-1}, in (b) for $v = 0.08$ mm^{-1}, in (c) for $v = 0.0$ mm^{-1}, respectively. The rest parameters of optical system are the same as those in Fig. 4.

3.3. Feasibility analysis in experiment

In practice, the actual patterns shown on the screen of SLM are digital, not continuous, which are discretely and numerically sampling in the modulation functions. The grating quality, as well as the intensity profiles generated in the focal plane, are influenced by the performance of digital display device, such as image resolution, size and gray level of each pixel, fill factor, refresh rates, and so on.

Equation (1) is the expression of the transmission function of ideal and spatial limited cosine grating. When this pattern is shown on the SLM with resolutions $M(x) \times N(y)$, equation (1) transforms into

$$\begin{aligned} g_{\mathrm{SLM}}(x,y) &= \cos(2\pi v x) \times \left[\mathrm{rect}\left(\frac{x}{\Delta H/\alpha}, \frac{y}{\Delta H/\alpha}\right) * \sum_{m=-M/2}^{M/2} \sum_{n=-N/2}^{N/2} \delta(x - m\Delta H, y - n\Delta H) \right] \\ &= \left[\cos(2\pi v x) \times \mathrm{rect}\left(\frac{x}{M\Delta H}, \frac{y}{N\Delta H}\right)\right] \times \left[\mathrm{rect}\left(\frac{x}{\Delta H/\alpha}, \frac{y}{\Delta H/\alpha}\right) * \frac{1}{\Delta H^2}\mathrm{comb}\left(\frac{x}{\Delta H}, \frac{y}{\Delta H}\right)\right] \\ &= g(x,y) \times t_{\mathrm{SLM}}(x,y), \end{aligned} \tag{4}$$

where we have used the assumption that the pixel sizes in x and y directions are of the same value, which is ΔH, to simplify our analysis, $M\Delta H = 2a$. The α is related with the fill factor of each pixel of SLM. The higher the fill factor is, the smaller α is. Especially, $\alpha = 1$ when fill factor is 100%. The t_{SLM} is decided by parameters of SLM, which is the convolution integral $(*)$ of the effective area of each pixel and a comb function. Equation (4) indicates that the digital grating is a product of the ideal one and t_{SLM}. So, the intensity distribution of the diffraction light field in the focal plane can be obtained from Fourier transformation of Eq. (4),

$$\begin{aligned} I_{\mathrm{SLM}}(x_0,y_0) &= I_f(x_0,y_0) * T_{\mathrm{SLM}}(x_0,y_0), \\ T_{\mathrm{SLM}}(x_0,y_0) &= \Im[t_{\mathrm{SLM}}(x,y)] \\ &= \frac{\Delta H^2}{(\lambda f)^2 \alpha^2} \sin c\left(\frac{\Delta H}{\alpha}\frac{x_0}{\lambda f}, \frac{\Delta H}{\alpha}\frac{y_0}{\lambda f}\right) \\ &\quad \times \mathrm{comb}\left(\Delta H\frac{x_0}{\lambda f}, \Delta H\frac{y_0}{\lambda f}\right). \end{aligned} \tag{5}$$

Thus, the effect of discrete sampling is equivalent to introduce a convolution factor of $T_{\rm SLM}$, which is a periodic comb function modulated by a sinc-function, into ideal intensity profile. It means that multi-order diffractions, which will reduce the quality of intensity profiles, are produced.

We first notice that the separation of different order diffraction is inversely proportional to $\Delta H/(\lambda f)$, which should not be smaller than the spread span of I_f to avoid mixing with each other. In the worst case, the ΔH should not larger than $1/(2v)$ by assuming that the spread span of I_f is approximately equal to the distance between the two optical wells. For current amplitude modulated SLMs, which offer pixel pitch of up to several microns, this separation can be estimated as $\sim$ 27 mm under typical data setting of $\Delta H = 20$ μm, $\lambda = 1.06$ μm and $f = 50$ cm. In our cases, the spatial scales of the multi-well traps, including optical lattices introduced in the next section, is about hundreds of microns, which is so small that the influence coming from other orders is tiny and can be ignored. Secondly, the factor $1/\alpha^2$ decides the efficiency of zero-order diffraction. Current fill factor for most commercial SLMs based on liquid crystal microdisplays can reach about 85%, and corresponding efficiency of zero-order diffraction is higher than 70%. The 100% fill factor is theoretically possible by using micro-lens arrays or special pixel structure, which has been realized on the reflection-type SLMs, such as the BNS (Boulder Nonlinear Systems, INC.) XY nematic series SLMs, and works on the transmission-type ones are also in progress.

It seems that the primary factor to make $I_{\rm SLM}$ different from I_f should be contributed to limited gray level of individual pixel on digital device, which results an imperfect sampling on $g(x, y)$. Though it is not considered in Eqs. (4) and (5), a numerical analysis has been performed by considering such effect, the results are shown in Fig. 6. The radial intensity distributions of I_f (solid line) and $I_{\rm SLM}$ (open circle) in focal plane are plotted in Fig. 6(a), in which we choose typical parameters of SLM with $\Delta H = 20$ μm, $\alpha = 1$ and gray level of 2^8. We notice that no significant difference between two profiles is presented unless magnification with three orders of magnitude is done. The absolute error $\Delta = |I_f - I_{\rm SLM}|$ is also shown in the same graph with close circles. The maximum of absolute error $\Delta_{\rm max}$ is 2.09×10^{-3} GW/m^{-2}, less than 2‰ of maximum of light intensity, and the mean value $\Delta_{\rm mean}$ is about 7.09×10^{-4} GW/m^{-2}, which is calculated by integrating over whole focal plane. Certainly, this error will increase with the reduction of gray level, but related error can be restricted in the range of $\leq 3\%$ as long as the gray level is greater than 2^6, see in Fig. 6(b).

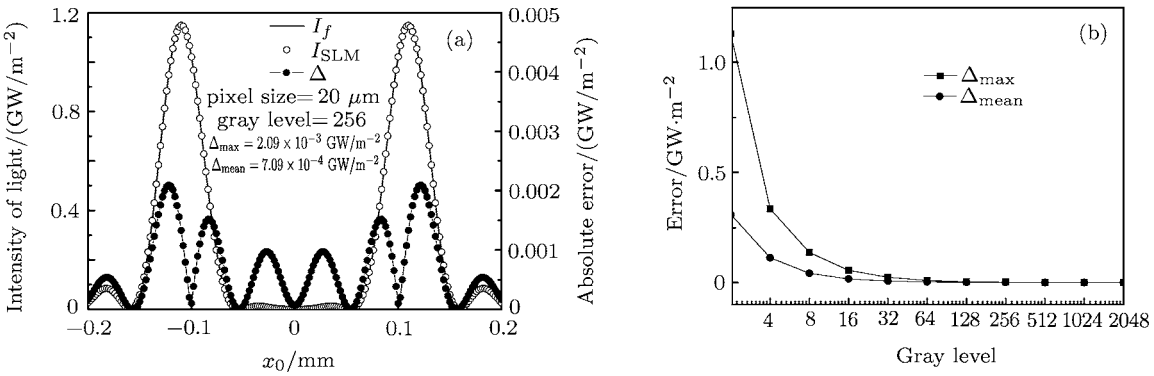


Fig. 6. (a) The radial intensity distributions of I_f (solid line) and $I_{\rm SLM}$ (open circle) in focal plane with $v = 0.2$ mm^{-1}. The absolute error $\Delta = |I_f - I_{\rm SLM}|$ is denoted by close circles. (b) The maximal (close rectangle) and mean error (close circles) depend on gray level of SLM.

Another problem encountered in practice of experiment is whether attainable refresh rate of current SLM met the requirement of dynamic control of cold atoms. By using common refresh rate of 80 Hz, we also performed a Monte-Carlo numerical simulation to show the dynamic loading process of cold ^{87}Rb atoms from the magneto-optical trap (MOT) into our single-well trap and the splitting process of cold atoms from a single well to a double one. This processes are shown in Fig. 7, in which the optical parameters are same as ones used in Fig. 5. In our simulation, a Gaussian cloud of atom with N=6×10^3 spin-polarized ^{87}Rb atoms in the hyperfine state

F = 2, $m_f = 2$ and temperature $T = 20$ μK is firstly prepared in the MOT, and then loaded them into our single-well optical trap ($v = 0.0$ mm^{-1}) for 500 ms. Figures 7(a) and 7(d) show atomic cloud in the x_0–y_0 and x_0–z planes, respectively. The initial half-width of atomic cloud is about 20 μm in three directions, which well match with the size of our single-well trap in x and y directions, but not in the third direction. As a result, a cigar-type cloud presents since obvious expansion presents in the z direction. Then, we change the parameter v from 0.0 mm^{-1} to 0.2 mm^{-1} during time of 2 s and refresh the optical field according 80 times per second. Figures 7(b) and 7(c) [or 7(e) and 7(f)] show the cases when $v = 0.1$ mm^{-1} and 0.2 mm^{-1}, respectively. In the end of splitting, two atomic clouds with separation of ~ 200 μm are evolved in the x direction. The atoms still held in our trap reach about 58.4% of initial number. Further studies show that this efficiency can be improved by using higher refresh rate or longer splitting time.

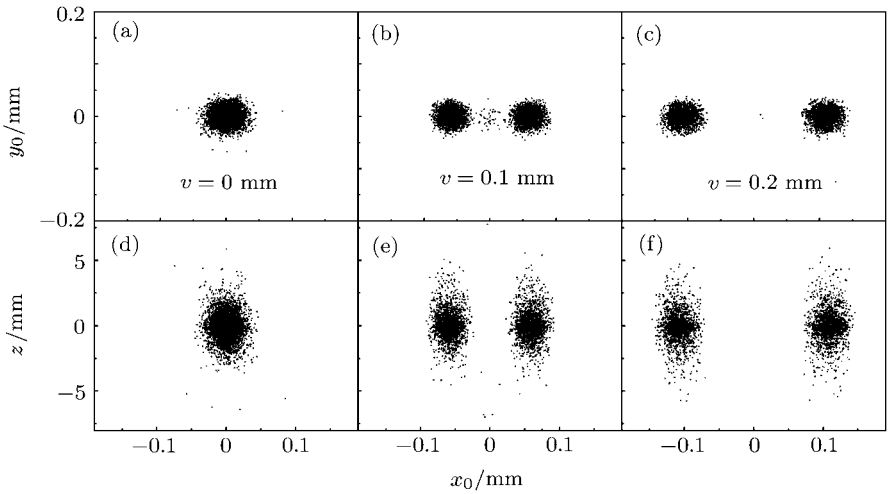


Fig. 7. Results of Monte-Carlo simulations: the evolution of cold atomic cloud in the x_0–y_0 [(a), (b), (c)] and x_0–z planes [(d), (e), (f)] during the loading and splitting processes of cold atoms.

4. Novel 2D optical lattices without using a microlens array

4.1. The case of using single-beam illumination

With the increase of the optical-well number in the x and y directions, a 1D or 2D array of optical microtraps will be formed, and the spatial periodicity of the lattices will play an important player in quantum and nonlinear atomic (or molecular) physics and atom (or molecule) optics. Here we firstly consider an orthogonally amplitude-modulated grating, its transmission is modulated along the two orthogonal directions and can be expressed as

$$\prod_N \cos(2\pi 2^{N-1} v_a x) \prod_M \cos(2\pi 2^{M-1} v_b y),$$

where v_a and v_b are the basic modulation frequencies along the x and y directions respectively. Generally, when $N \times M$ cosine functions are introduced into the diffraction integral, a 2D optical lattices containing $2^N \times 2^M$ uniform optical wells will be formed. In the case of using an orthogonal grating, we will obtain a 2D optical lattices with a rectangular lattice cell and the two orthogonal primitive translation vectors, $\boldsymbol{a} = 2v_a \lambda f \cdot \hat{x}$ and $\boldsymbol{b} = 2v_b \lambda f \cdot \hat{y}$, where $\hat{x}$ and $\hat{y}$ are the unit vectors along the x and y axes. Figure 8(a) shows an example of the 2D rectangular-cell lattice formed by our optical system with $v_a = 0.2$ mm^{-1} and $v_b = 0.1$ mm^{-1}. In the particular case of $v_a = v_b$, these two primitive vectors have equal lengths and corresponding lattices have higher rotational and reflective symmetries, which will lead to a 2D square-cell lattices, as shown in Fig. 8(b).

To obtain more novel types of 2D optical lattices with different lattice cells, we consider a non-orthogonally modulated grating, the two modulation directions have an arbitrary angle θ, one of them is chosen as the x axis. Then, the 2D modulation function of the grating should be changed to

$$\prod_N \cos(2\pi 2^{N-1} v_a x) \prod_M \cos[2\pi 2^{M-1} v_b (x \cos\theta + y \sin\theta)].$$

Although the diffraction integration in this case cannot be solved in an analytical form, we can still make sure two points: (i) the extension directions of the lattice cell is consistent with the modulation directions of the grating; (ii) the lattice constants still satisfy the relation given in Table 1. According to our numerical calculation, figure 8(c) shows a typical type of 2D oblique rectangular-cell lattices, where $\theta = 2\pi/5$, $v_a = 0.2$ mm^{-1}, $v_b = 0.3$ mm^{-1}, and the corresponding lattices constants are $|\boldsymbol{a}| = 0.212$ mm and $|\boldsymbol{b}| = 0.318$ mm, respectively. Additionally, another two types of 2D Bravais lattices can also be deduced. For example, when $\theta = \pi/3$ and $v_a = v_b$, the resulting lattice is a 2D triangular-cell (hexagonal-cell) one, as shown in Fig. 8(d). Another 2D optical lattices with a face-centred rectangular-cell lattices can be obtained when $\cos\theta = v_a/(2v_b)$, and its lattice microstructure is illustrated in Fig. 8(e).

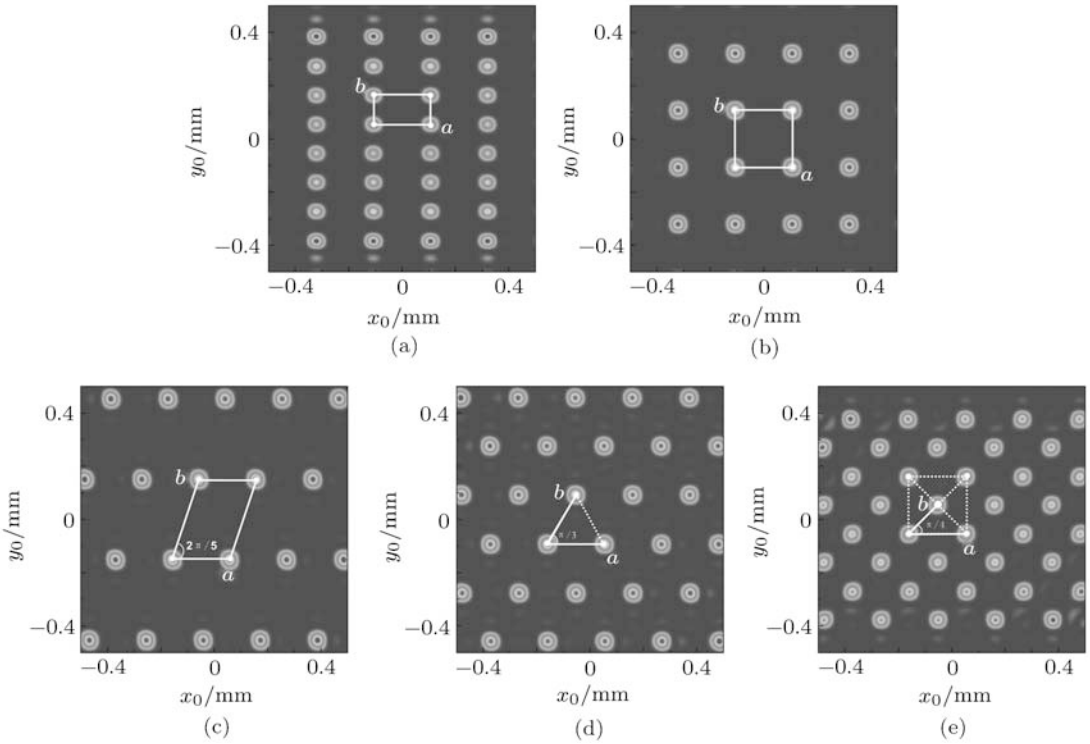


Fig. 8. Five types of 2D optical Bravais lattices formed by using orthogonal or non-orthogonal modulated grating: (a) rectangular-cell lattice; (b) square-cell lattice; (c) oblique-cell lattice; (d) triangular-cell lattice; (e) face-centred square-cell lattice.

In conventional standing-wave lattices, the geometrical structure of an optical lattice relies on lattice beam configuration, and the phase locking is significantly important to achieve stable phase contrast between the lattice beams. So a main advantage of our proposed lattice scheme is that various kinds of 1D or 2D lattices can be easily prepared by only using a simple optical system, which is composed of a single lens, a single-beam illumination and an amplitude-modulated cosine-only grating. Various grating patterns can be designed and optimized on a computer, and then the lattice configuration can be easily controlled and reconfigured by writing these patterns on the SLM in real time.

Furthermore, after forming 2D lattice, the separation between the adjacent two optical traps can be varied from several tens microns (the scale of single well's size in order to distinguish different optical wells) to a few hundreds microns. Such large transverse separation makes selectively address, initialization, and reading out the individual site become possible. On the other hand, if a lens with sufficient large relative aperture is applied, the transverse size of single well can be reduced to a smaller scale. It means that the lattices generated by our scheme can have a smaller lattice constant than ones generated by microfabricated optical systems,[20−22] and are expected to approach the scale of the standing-wave lattices. In

the regime of Fresnel diffraction, the permitted minimal focal length is about 15.4 mm for the half of the lens side-length $a = 5$ mm, i.e. the diffraction angle $\Omega \leq \pi/10$, and corresponding minimal lattice constant can be reduced into 1.45 μm. To obtain a smaller lattice constant, an appropriate correction on the diffraction of light field should be applied.

4.2. The case of using multi-beam illumination

To form more complex optical lattices, we now consider an incoherent multi-beam illumination with different incident angle. Such as, we use a plane light wave with an incident angle θ with respect to the z axis and an angle ϕ with respect to the zox plane to illuminate our optical system. In this case, an inclined phase factor of $\exp[\mathrm{i}\, 2\pi(x\sin\theta\cos\phi + y\sin\theta\sin\phi)]$ should be multiplied to the integrated function. However, we find that this phase factor can also be introduced into the integrated function by a coordination transformation with $z\sin\theta\cos\phi$ along the x' direction and $z\sin\theta\sin\phi$ along the y' direction, in which the integration form can keep unchanged. It means that the amplitude of the diffraction light field in the regime of slant incident beam can be expressed as $U(x' - z\sin\theta\cos\phi,\, y' - z\sin\theta\sin\phi,\, z)$. By using multi-beam illumination, we can prepare various compound lattices with a complex lattice cell, the two typical examples are shown below.

Figure 9(a) shows a scheme to obtain a 2D compound lattice with a square cell. In this scheme, an orthogonally amplitude-modulated grating with $v_a = v_b = 0.2$ mm^{-1} is used, and two incoherent beams with an incident angle $\theta = \pm v_a\lambda/2$ with respect to the oz axis and an angle $\phi = \pi/4$ with respect to the xoz plane is used to illuminate symmetrically our optical system [see the left configuration in Fig. 9(a)]. As a result, two square-cell lattices with a spatial separation of about 37.5 μm in x or y direction are generated in the focal plane of the lens, we call it a 2D compound lattice with a square cell. Especially, when $\theta = \sqrt{2}v_a\lambda/2$, one of the two lattices will be exactly located at the centre of another lattice and a face-centred square-cell structure is formed.

In Figure 9(b), we also give a three-beam illumination configuration in order to construct a lattice which contains periodic defects. In this case, one beam propagates along the oz axis, which will yield a square-cell lattice with a lattice constant of $2v_a\lambda f = 0.212$ mm, and another two beams propagate with an equal incident angle of $\theta = \arcsin(v_a\lambda)$ with respect to the oz axis in the zox and the zoy planes respectively, which will result in another two identical square-cell lattices with a displacement of 0.106 mm in x or y direction. As a result, these three sets of optical lattices are composed of a smaller 2D lattices with periodic defects, as shown in the right configuration of Fig. 9(b). The reducing lattices have a smaller lattice constant of 0.106 mm, but one site of a lattice cell is absent, which is regarded as a defect site, and the spatial period of defects is equal to 0.212 mm.

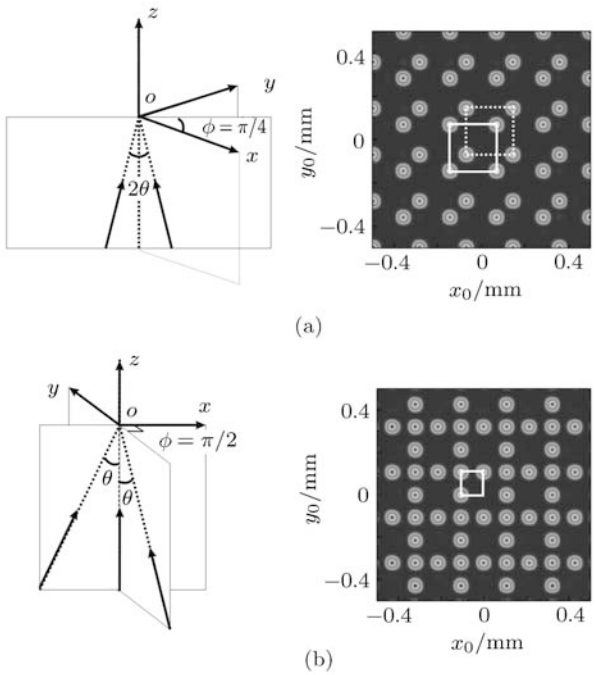


Fig. 9. Multi-beam illumination schemes. (a) A 2D compound lattice with a square cell, which is formed by two square-cell lattices. (b) A lattice with periodic defects, which is formed by three square-cell lattices.

Certainly, another alternative method to form an optical lattice is using a 2D array of micro-lenses to replace a single lens. In this scheme, each individual optical system is composed of a micro-lens and the corresponding amplitude-modulated region in the grating, which can be controlled even switched on or off independently.

Figure 10(a) shows the scheme to form a lattice with a double-well microtrap by using a 2D micro-lens array which contains 5×5 diffractive lens-lets with a focal length of $f = 600$ μm and a side length of $a = 200$ μm. The illuminating beam is derived from a 10-W Nd:YAG laser with a wavelength of $\lambda = 1.06$ μm and beam waist $w_0 = 1.414$ mm, which provides an average power of ~ 250 mW for each micro-lens, and

it perpendicularly passes through the grating modulated by a single cosine function with a frequency v along the x direction. When v= 0.01 μm^{-1}, the maximum intensity and the average intensity of each optical well are 25.3 GW/m^2 and 8.89 GW/m^2, respectively. The cigar-shaped trapping potential with a radial and axial geometric sizes of $\sim$ 1 μm and $\sim$ 10 μm is generated, which is a suitable aspect ratio (1:10) for an atomic cloud of Bose–Einstein condensation (BEC). After forming 2D lattice of double-well trap, the transverse separation between the adjacent two optical wells is determined by the separation of the micro-lens array, while the separation between two optical wells in individual cell depends only on the modulation frequency v, and a lattice of single-well trap can be created by reducing v to zero.

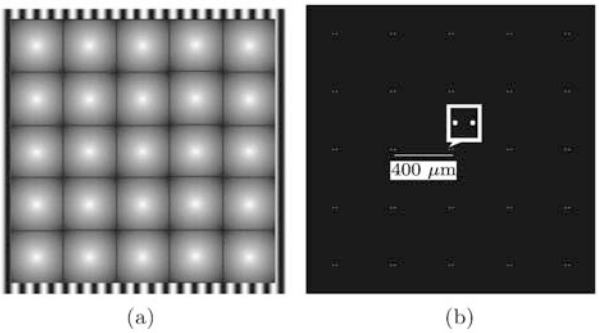


Fig. 10. (a) Scheme for a 2D optical lattice generated by a 2D array of 5×5 micro-lens with f = 600 μm and a = 200 μm. (b) A 2D optical lattice with 5×5 double-well traps for v = 0.01 μm^{-1}.

By increasing the number of modulation functions, we can obtain conveniently a 2D lattice of controllable multi-well traps, which will have an exciting prospect for all-optical BEC array and quantum information processing, which requires a smaller or adjustable spatial separation between the trapping potentials, e.g., quantum gate operations and the entanglement of ultracold atoms via atom–atom interactions.[12]

In addition to its flexibility, adopting a proper combination of the modulation functions and modulation frequency to increase the number of optical wells in individual cell and keep the separation unchanged, we can obtain a lattice with a cell number more than the micro-lens number. On the other hand, some overlapped traps between the two adjacent cells can also be created when the separation is further increased so as to exceed the micro-lens aperture. So, it is also possible to obtain a lattice containing site number less than the number of the micro-lens. Furthermore, non-uniform grating patterns can be applied in each cell, and result in an optical lattice with random lattice constants.

5. Conclusion

In this paper, we have discussed a new method to form a controllable optical multi-well trap or lattices for cold atoms or molecules by using amplitude cosine-only grating as a basic pattern element for a hologram. Our study shows that the characteristic parameters of each well is determined by the relative aperture of the lens and the wavelength of incident laser beam, while the separation between the two adjacent wells is related to the space frequency v of the cosine grating. Also, we have presented a continuous reversible evolution between a double-well trap and a single well. In addition, several approaches to expand our scheme to form various 2D novel optical lattices with a single- or multi-well optical trap have also been discussed. The proposed controllable multi-well traps and its multi-well lattices are expected to have some new and important applications in the fields of ultracold atomic physics and cold molecular physics, such as, some studies of cold collisions between multi-atomic or multi-molecular samples, the realization of all-optical atomic or molecular multi-well BEC and its multi-well BEC array, the preparation of novel 2D photonic crystals with cold atoms or molecules, and so on.

References

[1] Verkerk P, Lounis B, Salomon C, Cohen-Tannoudji C, Courtois J Y and Grynberg G 1992 *Phys. Rev. Lett.* **68** 3861

[2] Jessen P S, Gerz C, Lett P D, Phillips W D, Rolston S L, Spreeuw R J C and Westbrook C I 1992 *Phys. Rev. Lett.* **69** 49

[3] Blakie P B and Wang W X 2007 *Phys. Rev.* A **76** 053620-1

[4] Jochim S, Bartenstein M, Altmeyer A, Hendl G, Riedl S, Chin C, Hecker Denschlag J and Grimm R 2003 *Science* **302** 2101

[5] Yang R S and Yang J H 2008 *Chin. Phys.* B **17** 1189

[6] BenDahan M, Peik E, Reichel J, Castin Y and Salomon C 1996 *Phys. Rev. Lett.* **76** 4508

[7] Wilkinson S R, Barucha C F, Madison K W, Niu Q and Raizen M G 1996 *Phys. Rev. Lett.* **76** 4512

[8] Müstecaplıoğlu Ö E and Oktel M Ö 2005 *Phys. Rev. Lett.* **94** 220404-1

[9] Taşgın M E, Müstecaplıolu Ö E and Oktel M Ö 2007 *Phys. Rev.* A 75 063627-1

[10] Petrosyan D 2007 *Phys. Rev.* A **76** 053823-1

[11] Holmes M E, Tscherneck M, Quinto-Su P A and Bigelow N P 2004 *Phys. Rev.* A **69** 063408-1

[12] Jaksch D, Briegel H J, Cirac J I, Gardiner C W and Zoller P 1999 *Phys. Rev. Lett.* **82** 1975

[13] Song W 2009 *Chin. Phys.* B **18** 3251

[14] Shin Y, Saba M, Pasquini T A, Ketterle W, Pritchard D E and Leanhardt A E 2004 *Phys. Rev. Lett.* **92** 050405-1

[15] Zhou Q, Lu J F and Yin J P 2010 *Chin. Phys.* B **19** 093202

[16] Protsenko I E, Reymond G, Schlosser N and Grangier P 2002 *Phys. Rev.* A **65** 052301-1

[17] Amico L, Osterloh A and Cataliotti F 2005 *Phys. Rev. Lett.* **95** 063201-1

[18] Grier D G 2003 *Nature* **424** 810

[19] Bergamini S, Darquié B, Jones M, Jacubowiez L, Browaeys A and Grangier P 2004 *J. Opt. Soc. Am.* B **21** 1889

[20] Ji X M and Yin J P 2005 *J. Opt. Soc. Am.* B **22** 1737

[21] Lu J F, Ji X M and Yin J P 2006 *Chin. Opt. Lett.* **4** 683

[22] Dumke R, Volk M, Muther T, Buchkremer F B J, Birkl G and Ertmer W 2002 *Phys. Rev. Lett.* **89** 097903-1

[23] McGloin D, Spalding G, Melville H, Sibbett W and Dholakia K 2003 *Opt. Express* **11** 158

[24] Fatemi F K and Bashkansky M 2006 *Opt. Express* **14** 1368

[25] Rhodes D P, Gherardi D M, Livesey J, McGloin D, Melville H, Freegarde T and Dholakia K 2006 *J. Mod. Opt.* **53** 547

[26] Boyer V, Godun R M, Smirne G, Cassettari D, Chandrashekar C M, Deb A B, Laczik Z J and Foot C J 2006 *Phys. Rev.* A **73** 031402(R)-1

[27] Fatemi F K, Bashkansky M and Dutton Z 2007 *Opt. Express* **15** 3589

[28] Melville H, Milne G F, Spalding G C, Sibbett W, Dholakia K and McGloin D 2003 *Opt. Express* **11** 3562

[29] Barrett M D, Sauer J A and Chapman M S 2001 *Phys. Rev. Lett.* **87** 010404-1